Journal of Water Process Engineering 56 (2023) 104431

Contents lists available at ScienceDirect

Journal of Water Process Engineering

journal homepage: www.elsevier.com/locate/jwpe

Environmental remediation promoted by silver nanoparticles biosynthesized by eucalyptus leaves extract

Verónica Rocha [a,*], Pedro Ferreira-Santos [b], Zlatina Genisheva [c], Eduardo Coelho [a,d], Isabel C. Neves [a,e], Teresa Tavares [a,d]

[a] CEB - Centre of Biological Engineering, University of Minho, Campus de Gualtar, 4710-057 Braga, Portugal
[b] Department of Chemical Engineering, Faculty of Science, University of Vigo, As Lagoas, 32004 Ourense, Spain
[c] CVR – Centre for Wastes Valorisation, University of Minho, 4800-042 Guimarães, Portugal
[d] LABBELS - Associate Laboratory, Braga, Guimarães, Portugal
[e] CQ-UM - Centre of Chemistry, Department of Chemistry, University of Minho, Campus de Gualtar, 4710-057 Braga, Portugal

ARTICLE INFO

Keywords:
Green synthesis
Silver nanoparticles
Eucalyptus leaves
Antibacterial
Photodegradation

ABSTRACT

A simple and low-cost green synthesis method was optimized to prepare stable silver nanoparticles (AgNP) using aqueous *Eucalyptus globulus* leaves extract. This green method allows to obtain AgNP with spherical morphology and variable size around 25 nm, and it is dependent of the reaction temperature and concentration of the plant extract. AgNP stability was followed during 3 months by zeta potential measurements and a negative zeta range from −30.7 to −33.6 was determined. Biogenic-stabilized AgNP exhibited dual-functional properties as effective in environmental remediation with bacterial growth inhibition and dye photodegradation. *Staphylococcus aureus* and *Escherichia coli* were tested for antibacterial activity, and considerable inhibitory activity was found. High photocatalytic degradation of indigo carmine (IC) dye was performed in the presence of the AgNP as catalysts under sunlight irradiation. The degradation efficiency after 2 h of reaction was 37 %, 83 % and 98 % in the presence of UV light, visible light and sunlight irradiation, respectively. The germination of corn kernels test was used to determine the toxicity of the treated IC solutions and the results showed low toxicity after the photodegradation process.

1. Introduction

Demand for energy, materials and chemicals is growing due to the continuous growth of the global population combined with urbanization and industrialization [1]. A decreasing quality of the environmental systems is undoubtedly a consequence of releasing unwanted waste to the environment from many anthropogenic sources [2].

A variety of toxic dyes are used in the manufacture of leather, foodstuffs, paint, textile, plastic, paper, cosmetics, rubber and pharmaceuticals as a result of their exploitation leading to pollution of water resources which is dangerous for humans and the environment [3]. It is estimated that around 10,000 different types of synthetic and natural dyes are produced worldwide each year, weighing somewhere between 7×10^5 and 1×10^6 tons, with a significant amount of dyes wasted during the manufacturing and application processes [4,5]. The fixation of reactive dyes during the dying process is extremely inefficient, almost 50 % released directly into the environment [6]. The Indigo Carmine (IC) or Acid Blue 74 dye is extensively used as blue food additive, E132, and in the textile industry, and it is present as a pollutant in the major industrial effluents contaminating freshwater bodies [1]. The presence of two sulfonic acid groups in the molecule enhances its solubility in water [5]. IC dye is considered a highly toxic compound of the indigoid class of dyes and its direct contact causes skin and eye irritations, with permanent injury to the cornea and conjunctiva. It is also responsible for gastrointestinal irritations with nausea, diarrhea and vomiting [7,8]. As IC dye is very harmful to the environment even at low quantities, its removal from contaminated water is crucial.

Advanced oxidative processes (AOP) have been applied for wastewater treatment since the production of reactive free radicals allows to degraded organic pollutants by redox reactions [9]. Heterogeneous photocatalysis distinguishes out among AOP because it involves redox reactions induced by irradiation with catalysts. The ability to incorporate renewable sunlight energy in the form of solar photons is the main advantage of heterogeneous photocatalysis, which adds significant

* Corresponding author.
E-mail address: vrocha@ceb.uminho.pt (V. Rocha).

https://doi.org/10.1016/j.jwpe.2023.104431
Received 29 July 2023; Received in revised form 4 October 2023; Accepted 12 October 2023
Available online 17 October 2023

environmental value to the degradation process. In particular, for large-scale aqueous-phase applications, the use of solar light to photodegrade wastewater contaminants can make it a competitive method [10]. Recent reviews describe various catalysts that have been synthesized and used in wastewater treatment for degradation of dyes [11], PAH (Polycyclic Aromatic Hydrocarbons) [12], antibiotics [13] or herbicides [14]. IC was effectively degraded (87 %) under visible light by a heterostructured composite of borosilicate glass containing CdS/ZnS quantum dots [8]. Also, silver-attached reduced graphene oxide nanocomposite exhibited notable photocatalytic degradation ability towards both IC and methylene blue [15]. Sun et al. [16] studied the anthracene degradation by AgBr/BiOBr/TiO2 catalyst and founded a high photocatalytic activity, stability and adaptability of the new material.

Due to their excellent optical absorption over a broad range of the sunlight spectrum, including both visible light and UV light, noble metal nanoparticles (MNP) have been recognized as a type of effective media suitable for harvesting light energy for chemical processes [17]. Silver nanoparticles (AgNP) have gained much attention due to their excellent conductivity, stability and multiple applications as catalysts, antiviral, antifungal and antibacterial agents [18–21]. These remarkable properties of AgNP are attractive for heterogeneous catalysis, so they may be used as an efficient catalyst for clean-up of pollutants in liquid effluents.

For the synthesis of nanomaterials, there are several options, mostly categorized as physical and chemical methods. These conventional methods have limitations, such as their high energy demand and equipment supplies, production of flammable hydrogen gas and use of hazardous substances like $NaBH_4$, organic solvents, stabilizing and dispersion agents [22]. One of the most pressing needs in the field of environmental remediation is the development of a green, friendly, simple-to-implement, renewable and cost-effective method of MNP synthesis [1]. The research is focused on green synthesis of nanomaterials, avoiding the use of environmentally safe reactants and solvents and the absence of any unwanted byproducts during synthesis [23]. Cao et al. [24] synthesized carbon dots using yeast *Rhodotorula mucilaginosa* PA-1 and the carbon nanoparticle family showed very good potential to degrade malachite green under ultraviolet and visible light. In another work, a high photocatalytic efficiency of degradation of methylene blue using a composite of quantum dots and AuNP biosynthesized using the filamentous fungus *Phomopsis* sp. XP-8 [25]. A green nanocomposite of ZnO-MgO was produced using marine brown alga and showed a good photocatalytic degradation of Rhodamine B [26].

In the last two decades, there has been interest in the synthesis of MNP using plant extracts [18,27]. Plant extracts are utilized as reducing and capping agents for the biosynthetic formulation of these green nanomaterials. The features of the MNP generated are known to be influenced by the type of plant extract employed because different plant extracts contain varying quantities of organic reducing agents [28]. Eucalyptus, a genus in the *Myrtaceae* family, are the world's largest cultivated and natural hardwood flora [29]. Eucalyptus leaves extract has a high content of polyphenols, polyphenols, flavonoids, tannins terpenoids and monoterpenes that contribute to strong reducing ability [30]. In the first work on the eucalyptus-mediated synthesis of MNP, Ramezani et al. [31] used an extract of *Eucalyptus camaldulensis* as a reducing and capping agent for the synthesis of AuNP with size ranging from 1.25 to 17.5 nm. Until now, eucalyptus leaves extract has been used to biosynthesize different MNP such as ZnONP [23], FeNP [32], AgNP [33], CuONP [34], MgONP [35], Fe/NiNP [36] and Fe/PdNP [37], to be used in environmental remediation. Recently, ZnONP were synthesized from the leaf extract of *Eucalyptus grandis* and applied in the efficient photodegradation of tartrazine dye and as antimicrobial agent [38]. In the presence of biosynthesized FeNP by eucalyptus leaf extract, approximately 100 % of Cr(VI) was adsorbed [32]. Also, bimetallic Fe/NiNP biosynthesized with eucalyptus leaf extract showed a high catalytic activity in the degradation of methyl orange dye [36].

In this context, the present study aims to optimize and characterize the biosynthetic process of the green synthesis of AgNP using aqueous eucalyptus leaves extract from *Eucalyptus globulus*, a raw material from Portugal. The identification of the biomolecules involved in the AgNP synthesis was performed by HPLC-MS and GC–MS. The obtained AgNP were evaluated as environmental remediation agents (photocatalyst and antimicrobial). The main novelty of this study is the possibility of producing sustainable MNP through a green procedure, so they may be used in nanotechnological approaches for the degradation of harmful dyes and for the disinfection of pathogenic bacteria in liquid media.

2. Materials and methodologies

A detailed description of the materials and the methodologies used in this work are described in Supplementary Material.

2.1. Preparation of eucalyptus leaves extract

Eucalyptus leaves from *Eucalyptus globulus* were picked in Marco de Canaveses, Portugal (41°06′17.0″N 8°09′07.0″W) in September 2021. To remove impurities adhered, the collected fresh leaves were rinsed several times with distilled water and then dried at room temperature (RT) to constant weight. Dried leaves were chopped and ground to a fine powder (≤1 mm), in a mechanical grinder. Dried plant powder (25 g) was subjected to a conventional solid-liquid extraction using a cylindrical reactor into a water bath with shaking (200 rpm) and extracted with 250 mL of water at 50 °C for 30 min. Whatman filter paper No. 1 was used to filter the extract and the filtrate was stored at 4 °C for further use.

To determine the extraction yield, a glass slide was weighed and then 1000 µl of the extract was dropped on it, the weight of the slide and its content after evaporation (105 °C/12 h) was recorded. The yield was calculated take into account the weight of the powder sample, measured (25 g) by Eq. (1):

$$\text{Yield } (\%) = \frac{\text{Weight of aqueous extract (g)}}{\text{Weight of the powdered extract (g)}} \times 100 \quad (1)$$

2.2. Synthesis of AgNP using eucalyptus leaves aqueous extract: Preparation and characterization

Several amounts of eucalyptus leaves extract were added dropwise to $AgNO_3$ with constant stirring at different temperatures during 1 h. The resulting colored solution of AgNP was centrifuged and the precipitate was washed twice with distilled water and ethanol and then lyophilized (Fig. S1). The biosynthesized AgNP with 100 mL of extract at RT and 50 °C were labeled as $AgNP_{RT\text{-}1:1,}$ and $AgNP_{50°C\text{-}1:1}$, respectively, while the biosynthesized AgNP with 200 mL of extract at 50 °C were labeled as $AgNP_{50°C\text{-}1:2.}$

The AgNP were characterized by different techniques: Ultra-high Resolution Field-emission Scanning Electron Microscope (Auriga Compact, Zeiss) with a coupled microanalysis X-ray system (EDS - energy dispersive spectrometer); UV–Vis spectrophotometer; Fourier Transform Infrared Spectroscopy, X-ray photoelectron spectroscopy (XPS); Thermal gravimetric analysis (TGA); Dynamic light scattering (DLS) and X-ray diffraction (XRD).

2.3. Analytical methods for biomolecules identification

The identification of volatile compounds in the eucalyptus leaves extract was carried out using gas chromatography linked with mass spectrometry (GC–MS), was made according to Coelho et al. [39].

The identification of the polyphenolic compounds was made by HPLC equipped with MS/MS detector. More information is found in the Supplementary material.

The quantification of some phenolic compounds in aqueous extract of eucalyptus leaves, before and after synthesis of AgNP, was performed

using a Shimatzu Nexpera X2 ultra-performance liquid chromatography (UPLC) set-up, connected with Diode Array Detector (DAD) (Shimadzu, SPD-M20A), as described by Ferreira-Santos et al. [40]. All analyses were performed in triplicate.

2.4. Environmental remediation by AgNP

2.4.1. Evaluation of antibacterial activity

The antibacterial activity of the biosynthesized AgNP was evaluated using a traditional disc diffusion method. *Escherichia coli* (Gram-negative) and *Staphylococcus aureus* (Gram-positive) as sensitive bacteria were used and different amounts of AgNP were tested.

2.4.2. Evaluation of photocatalytic activity

The photocatalytic activity of biosynthesized AgNP on the degradation of IC as a wastewater pollutant model under UV light, visible light and sunlight irradiation, was evaluated during 2 h of reaction. The photodegradation reactions were carried out in a magnetically stirred photoreactor with an aqueous solution of IC (10 $mg{\cdot}L^{-1}$) dye with AgNP at RT, in dark condition over 30 min to allow the homogeneous dispersion. Thereafter, the solution was exposed to UV light irradiation and to visible light irradiation placed outside the reactor. The photocatalytic experiments under sunlight irradiation were conducted in an open space where it is possible to gather the solar radiation on a sunny day, between 12 a.m. and 2 p.m. Dye samples were withdrawn at fixed times, AgNP were separated from the dye solution through centrifugation and the supernatant was analyzed at 610 nm using a UV–Vis spectrophotometer.

The toxicity of the IC solution after 2 h of photodegradation under different irradiation was assessed by the germination of grains of corn kernels, based on a procedure adapted from Sancey et al. [41] and Tanji et al. [42]. 15 healthy grains of corn were placed in a Petri dish with two paper filters, and 5 mL of each aqueous solution was added every day: (A) Ultrapure water (control); (B) IC untreated solution at 10 $mg{\cdot}L^{-1}$; (C) IC solution after photodegradation under UV light irradiation; (D) IC solution after photodegradation under visible light irradiation, and (E) IC solution after photodegradation under direct sunlight irradiation, after 2 h of reaction. Petri dishes were covered and seeds were germinated in a growth chamber at RT in February of 2023. Three replicates were prepared for the assays.

The following equation is used to estimate germination after counting the number of seeds that have germinated after 7 days (Eq. (2)):

$$\text{Germination } (\%) = \frac{(\%\text{of germination control} - \%\text{of germination test})}{\%\text{of germination control}} \times 100 \quad (2)$$

3. Results and discussion

3.1. Optimization of the biosynthetic process of AgNP

The biosynthesis of AgNP is performed by reducing the Ag^{+} salt solution with the aqueous *Eucalyptus globulus* leaves extract, which was used both as a reducing and as a stabilizing agent (Fig. S1). The leaves obtained from trees at Marco de Canaveses, North of Portugal, are a by-product (bio-waste) of the lumber and cellulose industry. Several parameters influence the AgNP formation, such as reaction temperature and the concentration of the plant extracts [43,44]. Different temperatures (RT and 50 °C) and ratios between $AgNO_3$ and eucalyptus leaves extract (1:1 and 1:2) were tested. The color of the suspension progressively shifted to a dark brown, which indicated the formation of AgNP.

UV–Vis spectroscopy can be used as a useful method to recognize and characterize MNP [45]. The conduction electrons on the metal surface are set into their oscillations when MNP are exposed to light excitation. The resonance attained between the light photons and frequencies of surface electron oscillations is localized surface plasmon resonance (SPR). The green AgNP were analyzed in the wavelength range from 350 to 700 nm by UV–Vis. An individual spectral fingerprint for a plasmonic NP with a specific shape and size is produced by the wavelength for maximum absorption (λ_{max}) and band width [46]. Fig. 1A shows the optical spectra of AgNP, 1 h after the addition of the eucalyptus leaves extract at different synthesis conditions.

It can be seen in Fig. 1A that both AgNP obtained at 50 °C presents the characteristic SPR, with a λ_{max} at 458 and 464 nm for $AgNP_{50°C\text{-}1:1}$ and $AgNP_{50°C\text{-}1:2}$, respectively. These results confirm in a first approach, the successful synthesis of AgNP [47]. The broad peaks were also observed, indicating a broad size distribution. Similar results were obtained by other authors [45,48]. On the other hand, AgNP obtained at room temperature, $AgNP_{RT\text{-}1:1}$, do not show the characteristic SPR. Vimala et al. [49] that studied the effect of reaction temperature on the synthesis of AgNP using *Couroupita guianemsis*, showed that no AgNP could be formed under 37 °C during 60 min. Increasing the reaction temperature, the reduction rate also increases and the majority of Ag ions are consumed during the formation of nuclei, blocking the secondary reduction process on the surface of the produced nuclei [50].

Several publications claim to have successfully synthesized green AgNP at room temperature, but the incubation time is always longer than 1 h [45,48].

It is not possible to observe the AgNP formed at RT from the SEM analyses (Fig. 1C). This is in concordance with the obtained UV–Vis absorption spectra (Fig. 1A). Nevertheless, the synthesis at 50 °C showed the formation of AgNP with different shapes and sizes. With a low amount of extract ($AgNP_{50°C\text{-}1:1}$), the particles are irregularly shaped with a size distribution ranging from 42.9 to 142.9 nm (Fig. 1D). While the higher amount of extract ($AgNP_{50°C\text{-}1:2}$) results in the formation of particles with more defined shapes, mostly spherical, and the size distribution was in the range 58.0 to 101.4 nm (Fig. 1E). The calculated average particle size (average of 25 particles) suggests that the $AgNP_{50°C\text{-}1:1}$ have the largest one (84.1 ± 26.5 nm) and $AgNP_{50°C\text{-}1:2}$ have the smallest one (73.6 ± 10.9 nm). Due to their high surface energy, AgNP have a propensity to aggregate [43], so rapid nucleation in a short period of time is necessary to obtain monodispersed AgNP and for that, almost all ionic species have to be reduced rapidly and simultaneously to metallic species, followed by conversion to stable nuclei to be grown [51]. Zayed and Eisa [51] showed the influence of the concentration of extract in the biosynthesis of AuNP. The authors concluded that whereas faster nucleation produced monodisperse and smaller particles at the highest extract concentration, slower nucleation produced larger particles at the smallest extract volume, most likely as a result of a slower nucleation rate. Also, Baruah et al. [44] concluded that at high concentration of extract, sufficient reducing and capping agents become available which stabilize the growing nuclei and prevent the aggregation of particles. Pinto et al. [52], investigated the impact of different parameters on the morphology and size of AuNP and concluded that the concentration of extract plays a significant role.

FTIR analysis intend to reveal the structural differences between AgNP obtained at different synthesis conditions. Fig. 1B shows the representative spectra and clearly proves that no differences result from those conditions of biosynthesis. The stretching vibration of the N—H functional groups of the primary and secondary amines of amino acids, proteins and peptides is related with the large band at 2800–3500 cm^{-1} [53]. Additionally, the hydroxyl compounds (O—H) stretching vibration in aliphatic and phenolic structures are ascribed to this band [54]. The bands observed at 1721 cm^{-1} and 1612 cm^{-1} correspond to C═O functional group of carboxylic acid and C═C stretching vibrations of an aromatic alkene, respectively. Primary and secondary amides with N—H functional groups is related of the band at 1515 cm^{-1} [55]. The band at 1449 cm^{-1} is assigned to the C—H functional group of alkanes and the absorption bands in the region of 1357–1044 cm^{-1} represent the stretching of the C—O functional group of alcohols, carboxylic acids, esters and anhydrides [1]. The bands in the region of 922–608 cm^{-1} usually indicates the presence of out-of-plane C—H bending vibrations

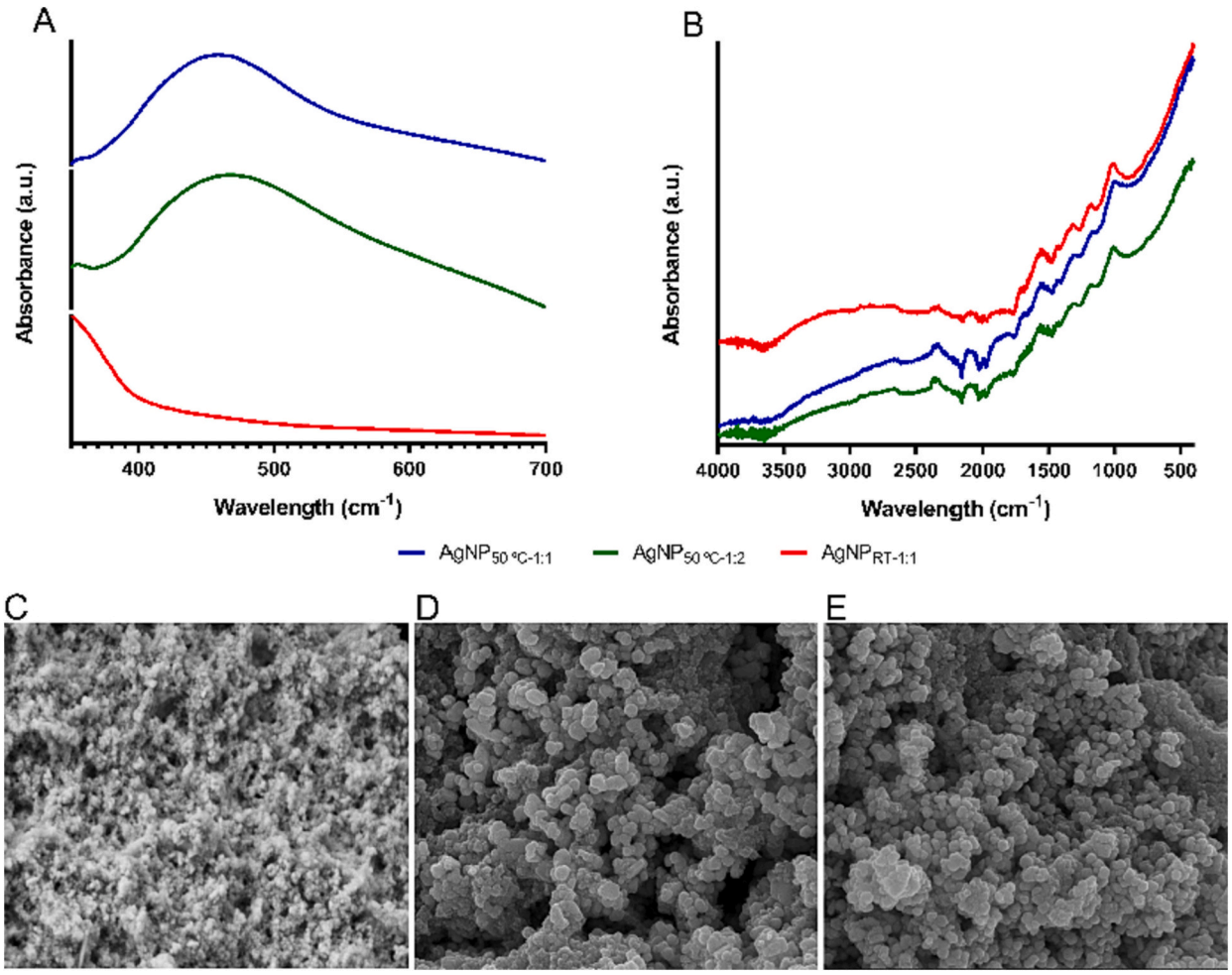

Fig. 1. Evaluation of optical properties by UV–Vis (A), functional structure by FTIR (B) and surface morphology and texture (C–E) by SEM of AgNP biosynthesized with eucalyptus leaves extract at different synthesis conditions: (C) $AgNP_{RT\text{-}1:1}$ at 30.00 k × magnification, (D) $AgNP_{50^{\circ}C\text{-}1:1}$ at 100,000 × magnification and (E) $AgNP_{50^{\circ}C\text{-}1:2}$ at 100,000 × magnification.

in alkenes and aromatics [20]. The presence of these bands provides confirmation that the AgNP is coated by phytochemicals from the eucalyptus leaves extract.

The surface composition, the relative distribution of elements and their oxidation state that are present on the surface of the $AgNP_{RT\text{-}1:1}$ and $AgNP_{50^{\circ}C\text{-}1:1}$ were assessed by X-ray photoelectron spectroscopy (XPS) measurements. Both samples revealed the presence of oxygen, carbon, nitrogen and chloride in their survey XPS resolution spectra, as well as silver in the region of Ag 3d (Fig. S2).

The binding energies (BE) of the elements as well as their amount (wt %) present on the surface, identified by XPS for both samples are shown in Table 1.

The values of the BE of the elements are similar between both samples, but the percentage of the elements are different, especially in the case of C 1s, Cl 2p and Ag 3d. The increase of the temperature in the preparation of AgNP affects the quantity of these elements on the surface. For $AgNP_{50^{\circ}C\text{-}1:1}$, the amount of carbon increases and the amount of chlorine and silver decreases, in comparison with the sample produced at room temperature. The higher amounts of carbon and oxygen are due to the biomolecules such as phenolic acids, flavones, flavonoids and others from eucalypts leaves extract. These findings suggest that elevated temperatures promote reactions among the biomolecule-derived compounds, leading to the formation of more complex structures. Moreover, the elements detected by the photoelectron peaks Cl 2p and N 1s can be attributed to compounds derived from biomolecules.

Table 1
Binding energies (BE) and the amount of the elements (wt%) from the XPS resolution spectra in the C 1s, O 1s, Cl 2p, N 1s and Ag 3d regions of the samples.

Sample		C 1s	O 1s	Cl 2p	N 1s	Ag 3d
$AgNP_{RT\text{-}1:1}$	BE (eV)	285.04	533.44	198.54	400.64	368.44
	Wt%	39.82	20.02	5.82	2.34	32.00
$AgNP_{50^{\circ}C\text{-}1:1}$	BE (eV)	286.40	533.80	198.50	400.30	368.90
	Wt%	52.07	24.28	1.97	2.19	19.48

The main carbon peak occurred at 285.04 and 286.40 eV for $AgNP_{RT\text{-}1:1}$ and $AgNP_{50^{\circ}C\text{-}1:1}$, respectively. For both samples, a deconvolution of the C 1 s peak revealed that carbon is present mainly as C—C, C—H, C—O and O=C-O groups from the biomolecules compounds, in accordance with the FTIR analysis. The O 1s peak was measured at 533.44 and 533.80 eV for $AgNP_{RT\text{-}1:1}$ and $AgNP_{50^{\circ}C\text{-}1:1}$, respectively, and the deconvolution revealed that the oxygen atoms are linked to the C present in the biomolecules (Fig. 2A and B).

Silver peak is measured at 368.44 and 368.90 eV for $AgNP_{RT\text{-}1:1}$ and $AgNP_{50^{\circ}C\text{-}1:1}$, respectively. In addition, silver amounts at the surface of each sample are different, with a decrease of Ag in the sample $AgNP_{50^{\circ}C\text{-}1:1}$ (Table 1). The deconvolution of Ag 3d peak (Fig. 2C and D) shows four peaks at the same BE for both samples, with an intense doublet corresponding to peak positions at 368.2 and 374.2 eV, for Ag $3d_{5/2}$ and Ag $3d_{3/2}$, respectively, with energy separations (Δ) of 6 eV, typical of metallic silver [56]. The other BE peaks located at 369.5 eV (Ag $3d_{5/2}$) and 375.4 eV (Ag $3d_{3/2}$) correspond to different silver species [56,57].

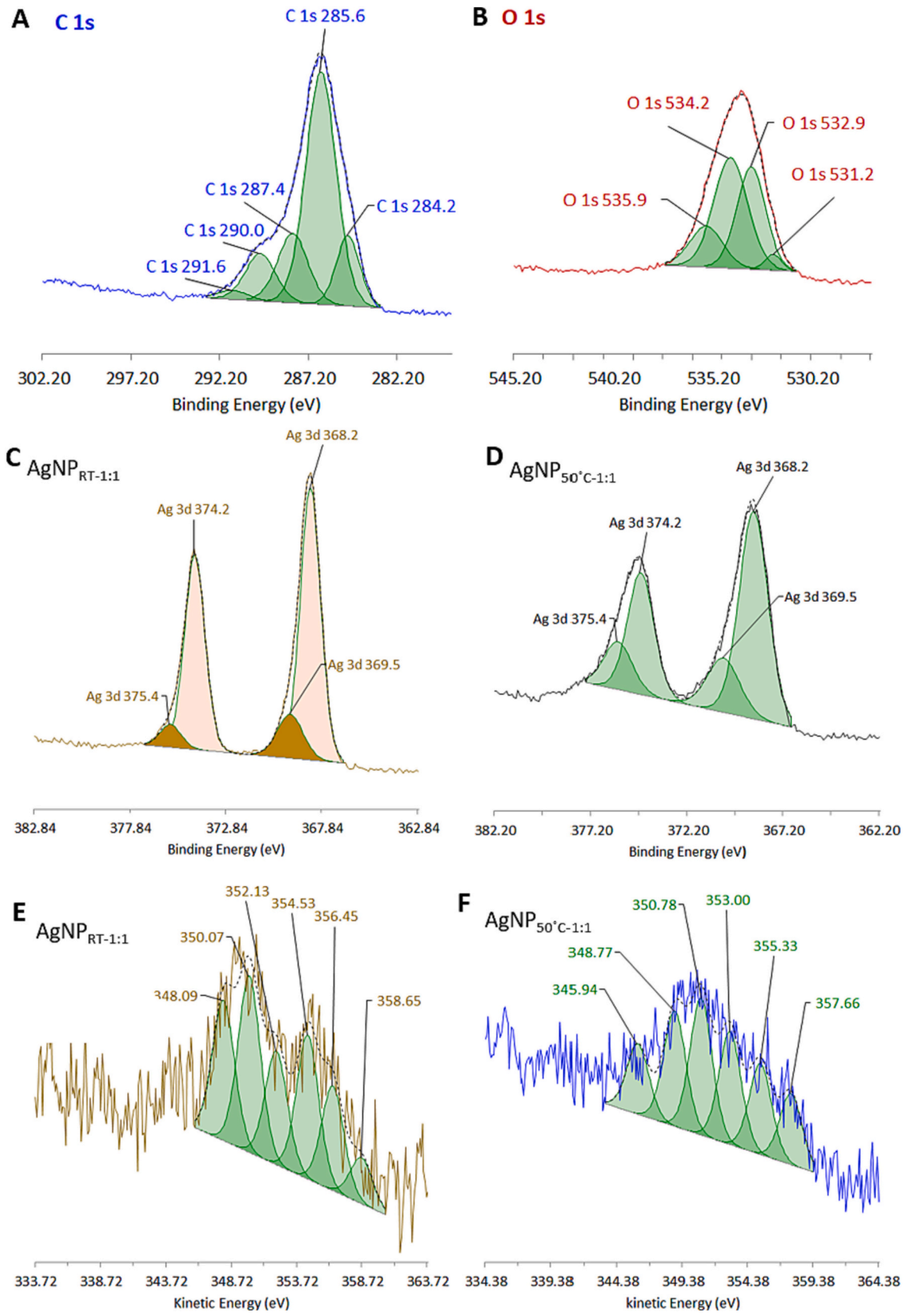

Fig. 2. High resolution XPS spectra of (A) C 1s and (B) O 1s from $AgNP_{50°C\text{-}1:1}$. (A) High resolution XPS spectra of Ag 3d region for (C) $AgNP_{RT\text{-}1:1}$ and (D) $AgNP_{50°C\text{-}1:1}$ and Auger spectra for (E) $AgNP_{RT\text{-}1:1}$ and (F) $AgNP_{50°C\text{-}1:1}$.

In order to identify the different silver species, the Auger spectra (Fig. 2E and F) were obtained for both samples, since the peak of Ag $3d_{5/2}$ displays two BE values at 368.2 eV and 369.5 eV, being difficult to distinguish the different chemical states due to the small chemical shift of the silver BE [58]. The Auger spectra obtained for both samples are similar between them with a complex form related to the Ag MNN regions with peaks assigned at different kinetic energy values. The sample $AgNP_{50°C\text{-}1:1}$ shows the same six peaks at lower values of kinetic energy compared to $AgNPs_{RT\text{-}1:1}$, with a contribution of different silver species. The presence of these species was defined by the Auger Parameter (AP) using BE (Ag $3d_{5/2}$) + KE (Ag MNN), where BE is the binding energy of Ag $3d_{5/2}$ peak (eV) and Ag MNN (KE) is the Auger kinetic energy [58]. Table 2 shows the values of kinetic energies, AP and the contribution of each silver species for both samples, according to the identification based on [57,59].

Different silver species were identified as Ag, Ag^+, AgO and Ag_2O, and they are dependent on the temperature used in the preparation of the AgNP. For the sample $AgNP_{RT\text{-}1:1}$, Ag^+ species is dominant with 64.3 % contribution, suggesting that the reduction of silver is not completed at this temperature, followed by 20.2 % of metallic Ag and 15.5 % of AgO. The increase in temperature changes the oxidation state of the same silver species and the presence of the silver oxide is improved with 38.2 % of AgO and Ag_2O, followed by only 19.3 % of Ag^+ and 42.6 % of Ag. At 50 °C, the silver reduction occurs and this indicates that increasing the amount of extract in the synthesis of AgNP at 50 °C can be sufficient to reduce the Ag^+ ions.

The thermal degradation of the $AgNP_{50\ °C\text{-}1:1}$ and $AgNPs_{50°C\text{-}1:2}$ was evaluated in order to understand the exclusive effect of the amount of extract on the synthesis of AgNP (Fig. 3A e B).

The first thermal event which occurred at temperatures of up to 75 °C and 91 °C showed 2.8 % and 3.1 % loss in weight of $AgNP_{50°C\text{-}1:1}$ and $AgNP_{50°C\text{-}1:2}$, respectively. This weight loss is attributed to the loss of water that has been adsorbed and is only weakly attached, as well as the loss of volatile substances in the extract, demonstrating that these substances exist and serve as biosurfactants for the AgNP [35,60]. The second weight losses (approximately 7 % and 10 %), which occurred at 243 °C and 299 °C, were a result of the thermal degradation of bioactive molecules containing carbon found on the surface of AgNP [60]. The weight loss observed between 300 °C and 800 °C may be due to the thermal degradation of phytoconstituents present on the AgNP, including the degradation of resistant aromatic compounds and the release of oxygen molecules present on the surface of the particles [61,62]. Finally, transitions were observed at above 800 °C for $AgNP_{50°C\text{-}1:2}$ and is close to the melting point of silver (961.78 °C). Thermal stability of $AgNP_{50°C\text{-}1:1}$ and $AgNP_{50°C\text{-}1:2}$ showed a weight loss <24 % and 26 %, respectively, up to 800 °C. These results suggest that the amount of extract to biosynthesize AgNP does not influence their thermal properties.

Zeta potential determinations allow estimation of the surface charge, which can be used to assess the physical stability of MNP [63]. A large positive or negative value of the zeta potential points out a good physical stability of the nanoparticles, due to the electrostatic repulsion between them. The zeta potential of the green AgNP determined in water as a dispersant was evaluated for 3 months and the results are shown in Fig. 3C, with the initial zeta potential values of -33.57 ± 0.19 and -32.33 ± 0.17 for $AgNP_{50°C\text{-}1:1}$ and $AgNP_{50°C\text{-}1:2}$, respectively. These values indicate that AgNP have a negatively charged surface, which implies strong repellent forces among the particles leading to aggregation prevention and stabilization of the AgNP in the medium. After 3 months, zeta potential values of -32.03 ± 0.49 and -31.50 ± 0.33 for $AgNP_{50°C\text{-}1:1}$ and $AgNP_{50°C\text{-}1:2}$ proved that the nanoparticles were stable.

XRD analysis is a popular technique used to investigate the crystal structure and size of MNP [29]. The XRD patterns of $AgNP_{50°C\text{-}1:2}$ were recorded from 20° to 80° as shown in Fig. 3D. The presence of the four distinct thin and narrow diffraction peaks in the XRD pattern indicates that synthesized AgNP are crystalline. These peaks at 38.10°, 44.29°, 64.44° and 77.38° are assigned to (1 1 1), (2 0 0), (2 2 0) and (3 1 1) *hkl* planes of face-centered cubic $AgNP_{50°C\text{-}1:2}$, respectively, in agreement with the other works (ICCD 00-001-1167 and JCPDS File N°:03-0921) [64,65]. Peaks at 27.84° and 32.19° are assigned to reflection planes of AgCl nanoparticles (ICCD 00-006-1480 and JCPDS File N°:00-031-1238) [66]. The other crystalline peaks (46.24° and 57.46°) are also observed and are due to the presence of organic compounds in the extracts [64,67,68]. Fig. S3 display the XRD patterns and ICDD file numbers of AgNP and confirm the presence of different Ag species in agreement with XPS analysis.

The crystallinity of the biosynthesized AgNP is 83.3 % and was calculated using the following equation (Eq. (3)):

$$\text{Crystallinity}\ (\%) = \frac{\text{Area of crystalline peaks}}{\text{Area of all peaks (crystalline + amourphous)}} \quad (3)$$

The average crystallite size of the synthesized NP was calculated using the Debye-Scherrer equation (Eq. (4)):

$$D = \frac{K\lambda}{\beta_D cos\theta} \quad (4)$$

where K is the Scherrer constant (0.94), λ is the X-ray wavelength (1.5421 Å), $\beta_D = \sqrt{\beta_m^2 - \beta_\alpha^2}$ where β_m is the width of the XRD peak at half-height (FWHM) and β_α is a constant determined from the instrument broadening (2.74×10^{-3} rad) and θ is the Bragg angle [48]. From the Scherrer equation, the average crystallite size of $AgNP_{50°C\text{-}1:2}$ is found to be 25.42 nm.

Table 2
Kinetic energies (KE), Auger Parameter (AP) and the contribution of the silver species in the Ag 3d region of the samples.

Sample			
KE (eV)	AP	Contribution (%)	Silver species
$AgNP_{RT\text{-}1:1}$			
356.64	724.84	15.53	AgO
354.11	722.31	17.35	Ag^+
351.15	719.35	23.69	Ag^+
348.78	716.98	23.21	Ag^+
359.87	728.07	7.59	Ag
345.99	714.19	12.63	Ag
$AgNP_{50°C\text{-}1:1}$			
355.33	723.53	15.27	AgO
353.00	721.20	18.90	Ag
350.78	718.98	22.88	Ag_2O
348.77	716.97	19.30	Ag^+
357.66	725.86	23.10	Ag
345.94	714.14	0.55	Ag

3.2. Identification of biomolecules in eucalyptus leaves extract

Eucalyptus globulus leaves extract was previously characterized chemically and selected as a promising candidate for the biosynthesis of AgNP by our research group. Eucalyptus leaves extract has been increasingly recognized as a rich source of bioactive molecules for the successful production of different NP [38,45,68]. In this work, the extraction yield was 18.4 (±0.1)% and similar results were obtained by Hassine et al. [69].

The biomolecules in the eucalyptus leaves extract were identified by different analytical techniques. It was possible to identify seventeen volatile compounds by GC–MS analysis of the aqueous extract of eucalyptus leaves (Table 3 and Fig. S4).

Most of the volatile compounds identified in the extract of these eucalyptus leaves were also described as constituents of other eucalyptus leaves. The major constituents of the *Eucalyptus globulus* leaves

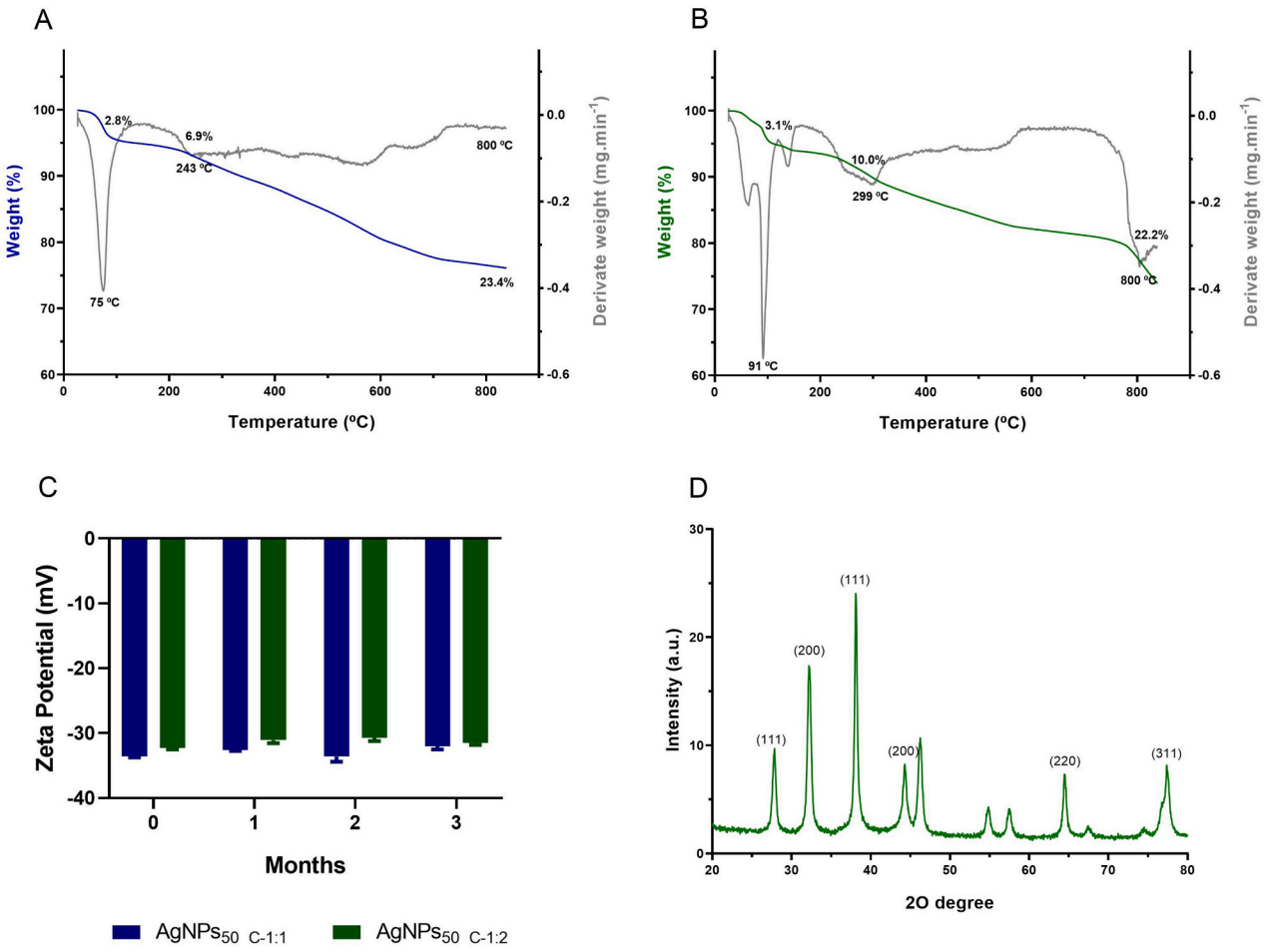

Fig. 3. Thermogravimetric analysis of (A) $AgNP_{50^{\circ}C\text{-}1:1}$ and (B) $AgNP_{50^{\circ}C\text{-}1:2}$; (C) Zeta potential evaluation during 3 months and (D) XRD pattern exhibiting the fcc structure of $AgNP_{50^{\circ}C\text{-}1:2}$.

extract were 1,8-cineole or eucalyptol (72.3 %), followed by pinocarveol (7.9 %) and pinocarvone (2.1 %). The concentration of other volatile compounds in such extract was <2 % (Table S1). 1,8-cineole was the most abundant, which is in good agreement with data reported by other studies [70–72]. Previous reports have shown the significance of these biomolecules in the synthesis of AgNP [46,73]. It was defended that sesquiterpenoids and monoterpenoids are the key donors for the synthesis of AgNP [74]. Wang et al. [75] identified the biomolecules of eucalyptus leaves extract involved in the formation of iron nanoparticles/reduced graphene oxide composites. The authors concluded that biomolecules such as 1,8-cineol, *trans-p*-mentha-1(7), *α*-terpineol, 8-dien-2-ol and *cis-p*-mentha-1(7), 8-dien-2-ol, due to their specific functional groups, a hydroxyl group (-OH) and =O, acted as reducing agents. Liu et al. [32] also identified specific biomolecules involved in the synthesis of iron nanoparticles, such as carveol, as reducing agent, and *α*-terpineol as capping agent. Ali et al. [76] demonstrated that terpenoids such as terpinen-4-ol and 1,8-cineole are involved in the formation of copper oxide nanoparticles. Based on these findings, it is forwarded that biomolecules such as (1) 1,8-cineol, (9) terpinen-4-ol (10) *α*-terpineol, (13) *trans-p*-mentha-1(7), 8-dien-2-ol, (14) carveol and (16) *cis-p*-mentha-1(7) are identified in literature as biomolecules in eucalyptus leaves that may contribute for the biosynthesis of MNP.

The phenolic profile of eucalyptus leaves obtained after aqueous extraction (Figs. S5 and S6) and the respective chemical identification are presented in Table 4. Fragmentation profiles were compared to the mass spectrometry database and literature to identify the compounds. Twelve phenolic compounds were detected, including flavonoids and phenolic acids. Some phenolic compounds of the eucalyptus leaves extract before and after synthesis of $AgNP_{50^{\circ}C\text{-}1:2}$ were quantified by HPLC with UV detection and are expressed in $mg{\cdot}L^{-1}$ (Table 4).

After synthesis of $AgNP_{50^{\circ}C\text{-}1:2}$, the amount of the compounds 3 (catechin), 5 (ellagic acid), 6 (rutin), 7 (gallic acid), 10 (quercetin) and 12 (kaempferol) decreased, and this decline was more accentuated for gallic acid, kaempferol and cathecin, with a reduction of 51, 31 and 26 %, respectively. These compounds can be used as reducing and/or capping agents in the reaction as stated in current works on gallic acid metal-reducing potential [65,77,78]. Santos et al. [65] observed that the concentration of gallic acid diminished after the synthesis of AgNP with eucalyptus bark extract and concluded that phenolic compounds, in particular derivatives of gallic acid, are mainly responsible for the metal-ion reduction. It is forwarded that AgNP may be synthesized upon the development of a transitory complex between Ag^{+} ions and the phenolic hydroxyl groups of the gallic acid. Subsequently, through the oxidation process, it changes to quinine that generates AgNP [77,78]. Other previous studies have shown that kaempferol [79] and quercetin [79,80] were able to reduce metal ions such as Ag^{+}. Based on the similarities between the AgNP synthesized using *Ocimum sanctum* leaves extract and pure quercetin in terms of optical, morphological and antibacterial properties, quercetin would be the main involved for the reduction of Ag^{+} ions [80]. Pradeep et al. [79] performed a systematic study to unveil the mechanism of synthesis of AgNP using extract of *Hypericum perforatum* and concluded that flavonoids and phenolic acids are involved in the reduction of Ag^{+} ions, phloroglucinols and xanthones act as capping agents and naphthodianthrones were responsible in both steps. Ghoreishi et al. [81] indicated that the –OH group of flavonoids (myricetin and quercetin) can be oxidized to carbonyl groups (-C=O) during the

Table 3
Identification of the volatile compounds present in aqueous extract of eucalyptus leaves.

Peak	Rt[a] (min)	Compound	% composition of the extract	Research on compounds identification
1	5.690	1,8-Cineole (eucalyptol)	72.30 ± 0.92	[69–72,75,76,95–100]
2	9.071	6-Methyl-5-hepten-2-one	<1	n.r.
3	10.562	(*Z*)-3-Hexenol	<1	n.r.
4	12.475	*cis*-Linalool furanic oxide	<1	n.r.
5	13.463	*trans*-Linalool furanic oxide	<1	[100]
6	16.470	Pinocarvone	2.14 ± 0.08	[72,99,100]
7	17.456	Fenchol	<1	[98–100]
8	17.977	Caryophyllene	<1	[72,98,100–102]
9	18.100	Terpinen-4-ol	<1	[72,76,95,98,102]
10	19.864	Pinocarveol	7.85 ± 0.20	[70,95,96,100]
11	21.594	*α*-Terpineol	1.16 ± 0.02	[32,72,75,76,97,98,100,102]
12	24.784	Myrtenol	<1	[95,99,102]
13	25.025	*trans-p*-Mentha-1(7),8-dien-2-ol	1.19 ± 0.02	[75,100]
14	26.414	Carveol	<1	[32]
15	26.863	*p*-Cymen-8-ol	<1	[100]
16	28.142	cis-*p*-Mentha-1(7),8-dien-2-ol	1.59 ± 0.02	[75,100]
17	28.706	2-Phenylethanol	<1	n.r.
18	33.936	Ledol	<1	[71,98,100]

[a] Rt = retention time (min); n.r. = not reported.

bioreduction of metal ions.

The mechanism of biological nanoparticle synthesis needs to be clarified through more detailed studies [79].

3.3. Environmental remediation of green AgNP

The environmental applications of green AgNP are focused in their potential as antimicrobial agents and as heterogeneous catalysts for the photodegradation of contaminants in aqueous effluents.

The antibacterial potential of MNP has been assessed and it may result from the production of reactive oxygen species (ROS), which destroy cell biomolecules and disrupt nuclear membranes and cells [82]. AgNP provide a broad spectrum of antimicrobial coverage, including bacteria, fungi and viruses. The antibacterial properties of synthesized $AgNP_{50°C\text{-}1:2}$ against two types of bacteria were investigated: *E. coli* (gram-negative) and *S. aureus* (gram-positive). The concentrations of AgNP in both cases ranged from 1.0 to 10.0 mg·mL^{-1} (Fig. 4).

The antibacterial activity of the $AgNP_{50°C\text{-}1:2}$ against *E. coli* and *S. aureus* can be evidenced in both cases, and the bacterial inhibition depends on AgNP concentration. The significant difference in the diameter of the zone of inhibition of the *S. aureus* and *E. coli* is detected with 1.0 mg·mL^{-1} of AgNP. The lower effect of AgNP against *S. aureus* is attributed to the difference in the bacteria membrane structure, distinctively: Gram-positive bacteria have a thicker cell wall made of peptidoglycan proteins, which allows them to gain resistance to AgNP, in contrast to Gram-negative bacteria, which have weaker cell walls. Since Gram-positive bacteria have negatively charged cell walls that can draw silver ions to their surface, it is possible to reduce the number of silver ions that reach the plasma membrane [83]. Bhuyan et al. [84]

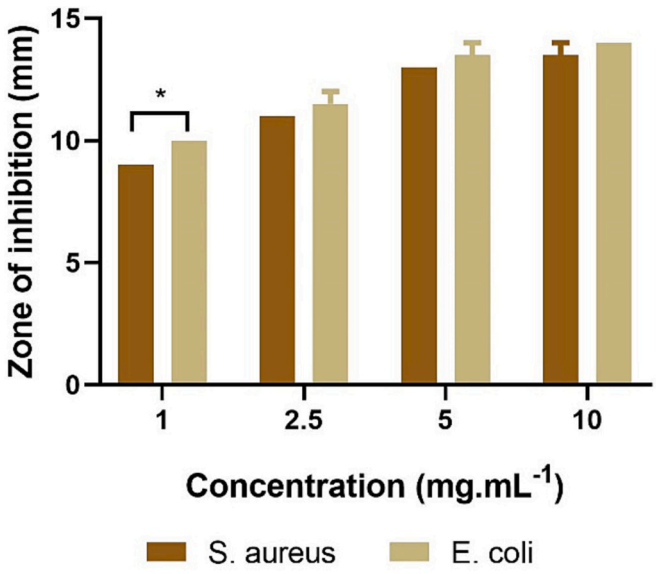

Fig. 4. Antibacterial activity of $AgNP_{50°C\text{-}1:2}$ at range concentration 1–10 mg·mL^{-1}. The symbol * shows significant differences ($p < 0.05$) between inhibition zone of the same concentration of AgNP in different bacteria.

Table 4
HPLC-MS fragmentation profile and abundance of phenolic compounds identified in eucalyptus leaves extract before and after AgNP synthesis.

Peak no.	Rt[a] (min)	$[M\text{-}H]^-$ [*m/z*]	MS^n product ions [*m/z*]	Compound	Quantification of phenolic compounds in eucalyptus leaves extract [mg·L^{-1}]		Research on compounds identification
					Before AgNP synthesis	After AgNP synthesis	
1	7.49	191	173, 111, 87, 85	Quinic acid	–	–	[102]
2	8.33	353	191	Chlorogenic acid	–	–	[102–107]
3	9.23	289	245, 205, 203, 125, 109	Catechin	232.6 ± 12.4	172.2 ± 10.7	[106]
4	12.4	635	483, 465, 313, 211, 169	Trigalloyl-glucoside	–	–	[108,109]
5	13.73	301	229, 185, 173, 157, 146	Ellagic acid	250.1 ± 3.6	209.0 ± 2.2	[102,103,107,109]
6	13.83	610	301	Rutin (quercetin-3-O-rutinoside)	266.3 ± 3.5	239.8 ± 1.8	[104,105]
7	13.93	169	125	Gallic acid	165.7 ± 2.1	79.6 ± 0.8	[102,103,106,107,109,110]
8	14.65	433	243, 271, 300	Quercetin 3-arabinoside	–	–	[102]
9	15.36	463	151, 179, 301	Spiraeoside	–	–	n.r.
10	17.36	301	179, 165, 151, 121, 107	Quercetin	2.4 ± 0.2	2.100 ± 0.003	[104,110]
11	18.64	395	305, 275, 247	8-Glucosyl-5,7-dihydroxy-2-(1-methylpropyl)chromone	–	–	n.r.
12	18.69	285	–	Kaempferol	17.2 ± 1.0	11.9 ± 0.8	[102,103]

[a] Rt = retention time (min); n.r. = not reported.

reported that the superficial contact of AgNP with the cell membrane can inhibit enzymatic systems of the respiratory chain, the replication of bacterial DNA is reduced and inactivation of protein occurs. The results obtained with green synthesized AgNP are consistent with the well-known powerful antibacterial properties of AgNP [80,85].

Recent studies have shown that green AgNP can be used as heterogeneous catalyst in the photodegradation of a variety of dyes [1,33]. The mechanism of photodegradation of dyes by MNP is attributed to the formation of surface plasmons in the MNP under photonic excitation. This photo absorption process is followed by the creation of electrons, transfer of charge carriers and recombination of charge carriers with the organic dye molecules after this excitation step activates the dye [86]. The band gap energy (E_g) is an essential parameter determining the performance of the photocatalyst [80,87]. The corresponding band gap value of $AgNP_{50°C\text{-}1:2}$ could be estimated according to Eq. (5):

$$E_g = \frac{1240}{\lambda_g} \quad (5)$$

E_g is the band gap of the AgNP and λ_g is the threshold wavelength, the one of the corresponding absorbance edge [87]. The estimated E_g was 2.67 eV, making it able to participate effectively in the photodegradation of pollutants [88].

Here, the photodegradation activity of biosynthesized $AgNP_{50°C\text{-}1:2}$ is evaluated using a model dye molecule, IC (Fig. 5A). This performance parameter was monitored over time by UV–visible spectroscopy at 610 nm, during 2 h of reaction. To demonstrate the efficiency of biosynthesized AgNP and the impacts of different irradiations on the IC degradation, control experiments were carried out.

The results indicate that the removal of IC is insignificant under UV light, visible light and sunlight irradiations without the presence of AgNP in line with other works [89]. In addition, no significant changes are observed during the dye degradation experiment conducted in the dark in the presence of AgNP. These data confirm that the dye degradation rely on both the presence of AgNP and the irradiation as in a typical heterogeneous photocatalysis. The absorption peak of IC dye (610 nm) decrease with the increase in irradiation time and almost disappears at the end of reaction (Fig. S7) evidencing the extinction of the molecular structure of the IC dye by an attack on the exocyclic double bond [89,90]. After 60 min, 93.8 ± 0.6 % of the IC dye is degraded under sunlight irradiation, whereas only 27.4 ± 1.5 % and 18.8 ± 2.4 % degradations are reached under visible and UV light, respectively. These results are also confirmed by the kinetic analysis that determined that the photocatalytic decolorization of IC is fitted by a pseudo first-order kinetic model (Eq. (6)):

$$ln\frac{C}{C_0} = -k \cdot t \quad (6)$$

C_0 is the IC dye initial concentration, C is the concentration of IC dye at t (time) and k (min^{-1}) is the apparent rate constant.

The plot of ln (C/C_0) vs time for the photocatalytic degradation of the IC dye solution using $AgNP_{50°C\text{-}1:2}$ is shown in Fig. 5B. The k calculated is found to be 0.0476, 0.0152 and 0.0039 min^{-1} for sunlight, visible and UV light, respectively, and confirms that sunlight is the best radiation to promote the photodegradation. The regression coefficient values are higher than 0.933, which indicates that the experimental data are well fitted by the pseudo-first-order model (Table 5). The half-life ($t_{1/2}$) of the decolorization is calculated using Eq. (7):

$$t_{1/2} = \frac{0.693}{k} \quad (7)$$

The half-life is found to be 14.56, 45.59 and 177.69 min for IC decolorization under sunlight, visible and UV light, respectively.

A possible mechanism for the photodegradation of IC dye includes the absorption of photons of energy that release electrons in the conduction band and generates holes in the valence band. The photogenerated holes formed in the valence band migrate closer to the IC dye molecules and take part in the oxidative photodegradation by

Table 5
Values of decolorization efficiency (%), kinetic constant (k = min^{-1}) and linear correlation coefficient (R^2) for IC photodegradation under UV, visible and sunlight irradiation.

Radiation type	Decolorization efficiency %	Rate constant (k, min^{-1})	Squared R (R^2)
UV	37.41 ± 4.12	0.0039	0.9942
Vis	83.30 ± 2.03	0.0152	0.9311
Sunlight	97.58 ± 0.51	0.0476	0.9821

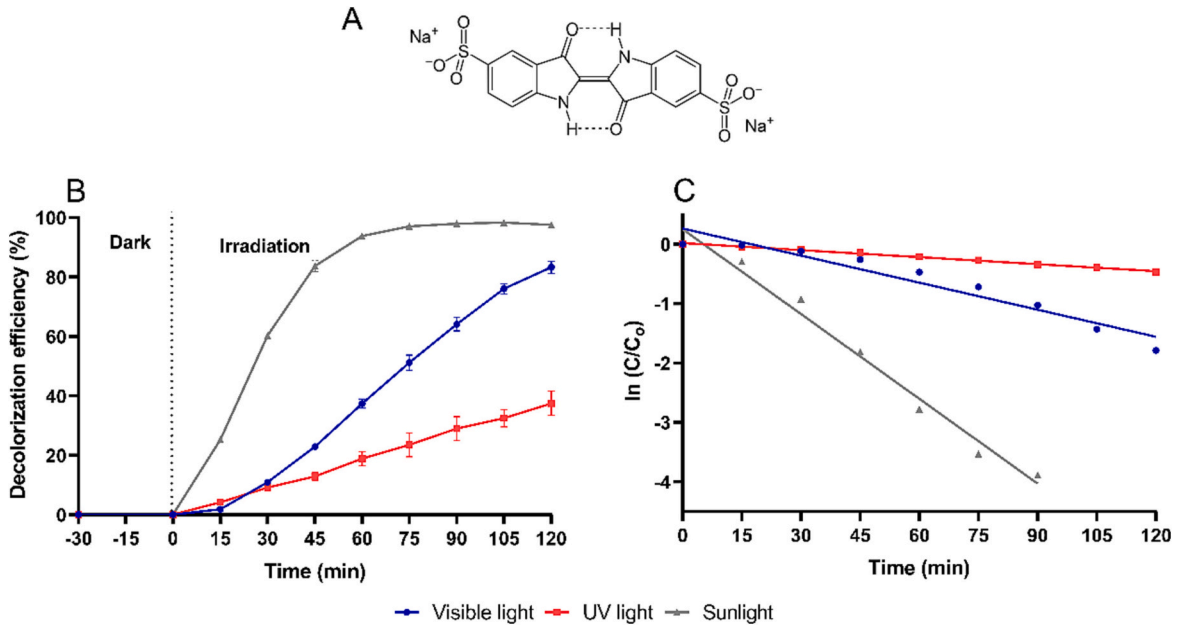

Fig. 5. Evaluation of photocatalytic efficiency of $AgNP_{50°C\text{-}1:2}$ under different irradiations (A) Indigo Carmine (IC) dye, (B) Decolorization efficiency vs time and (C) ln (C/C_0) vs time. (For interpretation of the references to color in this figure legend, the reader is referred to the web version of this article.)

producing hydroxyl radicals (•OH) from adsorbed water molecules. The photo-generated electrons from the conduction band are captured by adsorbed molecular oxygen on the surface of the AgNP and become superoxide free radicals [15,91,92]. The total mineralization is not confirmed in this work. However, some previous investigations [93,94] showed the photodegradation of IC dye into isatin sulfonic acid up to 2-amine-5-sulfo-benzoic acid formation via oxidation.

These comparative evaluations demonstrated that direct sunlight irradiation is the optimum condition for the photocatalytic reduction of IC dye in presence of AgNP. Solar energy for the degradation of pollutants by photocatalysis is an economic and sustainable solution.

For the evaluation of the phytotoxic effect of the treated solution after photodegradation, germination tests with corn kernels were performed (Fig. S8).

There is a significant difference between the untreated solution (control) and treated IC solutions by photodegradation using $AgNP_{50°C1:2}$ catalyst. The germination of corn kernels was assessed in Petri dishes irrigated with ultra-pure water during 7 days at room temperature. The assays were performed in February 2023, and the temperature of the water was 15 °C. The germination of corn kernels was successful in control (70 %).

On the other hand, the germination was minor for untreated aqueous solutions containing IC dye at 10 $mg{\cdot}mL^{-1}$, which did not exceed 13 %, and treated solutions under UV, visible light and sunlight irradiation reached in 7 days 40, 53 and 73 %, respectively. In presence of sunlight irradiation, the germination is similar to the control. This confirms low phytotoxicity after the photocatalytic degradation processes mainly with sunlight radiation, the results of phytotoxicity being in agreement with the results of photodegradation. Consequently, degradation catalyzed by AgNP and under sunlight irradiation reached the best combination for preventing or decreasing the environmental impact of the contaminated effluents by dyes.

4. Conclusions

Natural resources have created numerous opportunities for the green synthesis of MNP. Leaves from *Eucalyptus globulus*, a raw plant in Portugal are inexpensive, locally available, abundant and eco-friendly. These eucalyptus extracts revealed to be an excellent resource for the synthesis of stable AgNP with a significant impact on the environment by reducing waste and producing benefits for the MNP. The reaction temperature and concentration of the eucalyptus leaves extract affected the AgNP synthesis and the best results were obtained at 50 °C and a ratio 1:2. $AgNP_{50°C1:2}$ showed a spherical shape with high stability and a pure crystalline nature with an average crystallite size of 25.42 nm. Biomolecules identified as being in eucalyptus as catechin, ellagic acid, rutin, gallic acid, quercetin and kaempherol were used as reducing and/or capping agents in the synthesis of AgNP. These nanoparticles exhibited efficient antibacterial activity against both gram-positive and gram-negative bacteria: *Escherichia coli* (15 mm maximum zone of clearance) and *Staphylococcus aureus* (14 mm maximum zone of clearance). High photodegradation of IC dye under UV, Visible light and sunlight radiation was successfully achieved with sunlight as the best compromise. In addition, germination tests confirmed the efficiency of the IC photodegradation using AgNP with sunlight radiation. This work is promoting the development of a dual-in-one platform for cleaning up wastewater systems.

Declaration of competing interest

The authors declare that they have no known competing financial interests or personal relationships that could have appeared to influence the work reported in this paper.

Data availability

The authors are unable or have chosen not to specify which data has been used.

Acknowledgements

V.R. thanks to Fundação para Ciência e Tecnologia, FCT (Portugal) for her Ph.D. grant (SFRH/BD/141073/2018). P·F-S. would like to express their gratitude to the Spanish Ministry of Economy and Competitiveness for their postdoctoral grant (Reference FJC2021-046978-I). This research work has been funded by FCT/MCTES (PIDDAC) over the projects: CQ-UM (UID/QUI/0686/2020), CEB (UIDB/04469/2020) and LABBELS (LA/P/0029/2020), and project BioTecNorte (operation NORTE-01-0145-FEDER-000004), supported by the Northern Portugal Regional Operational Program (NORTE 2020), under the Portugal 2020 Partnership Agreement, through the European Regional Development Fund (ERDF).

Appendix A. Supplementary data

Supplementary data to this article can be found online at https://doi.org/10.1016/j.jwpe.2023.104431.

References

[1] P. Rani, V. Kumar, P.P. Singh, A.S. Matharu, W. Zhang, K.-H. Kim, J. Singh, M. Rawat, Highly stable AgNPs prepared via a novel green approach for catalytic and photocatalytic removal of biological and non-biological pollutants, Environ. Int. 143 (2020), 105924, https://doi.org/10.1016/j.envint.2020.105924.
[2] H. Ali, E. Khan, I. Ilahi, Environmental chemistry and ecotoxicology of hazardous heavy metals: environmental persistence, toxicity, and bioaccumulation, J. Chem. 2019 (2019), 6730305, https://doi.org/10.1155/2019/6730305.
[3] F. Luo, D. Yang, Z. Chen, M. Megharaj, R. Naidu, One-step green synthesis of bimetallic Fe/Pd nanoparticles used to degrade Orange II, J. Hazard. Mater. 303 (2016) 145–153, https://doi.org/10.1016/j.jhazmat.2015.10.034.
[4] E. Errais, J. Duplay, F. Darragi, I. M'Rabet, A. Aubert, F. Huber, G. Morvan, Efficient anionic dye adsorption on natural untreated clay: kinetic study and thermodynamic parameters, Desalination 275 (2011) 74–81, https://doi.org/10.1016/j.desal.2011.02.031.
[5] M.F. Chowdhury, S. Khandaker, F. Sarker, A. Islam, M.T. Rahman, M.R. Awual, Current treatment technologies and mechanisms for removal of indigo carmine dyes from wastewater: a review, J. Mol. Liq. 318 (2020), 114061, https://doi.org/10.1016/j.molliq.2020.114061.
[6] A. Telke, D. Kalyani, J. Jadhav, S. Govindwar, Kinetics and mechanism of reactive red 141 degradation by a bacterial isolate rhizobium radiobacter MTCC 8161, Acta Chim. Slov. 55 (2007).
[7] M.F. Abdel Messih, M.A. Ahmed, A. Soltan, S.S. Anis, Facile approach for homogeneous dispersion of metallic silver nanoparticles on the surface of mesoporous titania for photocatalytic degradation of methylene blue and indigo carmine dyes, J. Photochem. Photobiol. A Chem. 335 (2017) 40–51, https://doi.org/10.1016/j.jphotochem.2016.11.001.
[8] S.Y. Janbandhu, S. CT, S.R. Munishwar, J.R. Jayaramaiah, R.S. Gedam, Borosilicate glasses containing CdS/ZnS QDs: a heterostructured composite with enhanced degradation of IC dye under visible-light, Chemosphere 286 (2022), 131672, https://doi.org/10.1016/j.chemosphere.2021.131672.
[9] S.O. Ganiyu, S. Sable, M. Gamal El-Din, Advanced oxidation processes for the degradation of dissolved organics in produced water: a review of process performance, degradation kinetics and pathway, Chem. Eng. J. 429 (2022), 132492, https://doi.org/10.1016/j.cej.2021.132492.
[10] M.E. Borges, M. Sierra, E. Cuevas, R.D. García, P. Esparza, Photocatalysis with solar energy: sunlight-responsive photocatalyst based on TiO2loaded on a natural material for wastewater treatment, Sol. Energy 135 (2016) 527–535, https://doi.org/10.1016/j.solener.2016.06.022.
[11] V. Gadore, S.R. Mishra, M. Ahmaruzzaman, Metal sulphides and their heterojunctions for photocatalytic degradation of organic dyes-a comprehensive review, Environ. Sci. Pollut. Res. 30 (2023) 90410–90457, https://doi.org/10.1007/s11356-023-28753-w.
[12] O. Samuel, M.H.D. Othman, R. Kamaludin, H. Dzinun, A. Imtiaz, T. Li, T. El-badawy, A.U. Khan, M.H. Puteh, E. Yuliwati, T.A. Kurniawan, Photocatalytic degradation of recalcitrant aromatic hydrocarbon compounds in oilfield-produced water: a critical review, J. Clean. Prod. 415 (2023), 137567, https://doi.org/10.1016/j.jclepro.2023.137567.
[13] A. Azimi-Fouladi, P. Falak, S.A. Hassanzadeh-Tabrizi, The photodegradation of antibiotics on nano cubic spinel ferrites photocatalytic systems: a review, J. Alloys Compd. 961 (2023), 171075, https://doi.org/10.1016/j.jallcom.2023.171075.

[14] M.H. Hazaraimi, P.S. Goh, W.J. Lau, A.F. Ismail, Z. Wu, M.N. Subramaniam, J. W. Lim, D. Kanakaraju, The state-of-the-art development of photocatalysts for the degradation of persistent herbicides in wastewater, Sci. Total Environ. 843 (2022), 156975, https://doi.org/10.1016/j.scitotenv.2022.156975.
[15] P.P.A. Jose, M.S. Kala, N. Kalarikkal, S. Thomas, Silver-attached reduced graphene oxide nanocomposite as an eco-friendly photocatalyst for organic dye degradation, Res. Chem. Intermed. 44 (2018) 5597–5621, https://doi.org/10.1007/s11164-018-3443-8.
[16] X. Sun, W. He, X. Hao, H. Ji, W. Liu, Z. Cai, Surface modification of BiOBr/TiO2 by reduced AgBr for solar-driven PAHs degradation: mechanism insight and application assessment, J. Hazard. Mater. 412 (2021), 125221, https://doi.org/10.1016/j.jhazmat.2021.125221.
[17] S. Sarina, E.R. Waclawik, H. Zhu, Photocatalysis on supported gold and silver nanoparticles under ultraviolet and visible light irradiation, Green Chem. 15 (2013) 1814–1833, https://doi.org/10.1039/C3GC40450A.
[18] S.S. Salem, A. Fouda, Green synthesis of metallic nanoparticles and their prospective biotechnological applications: an overview, Biol. Trace Elem. Res. 199 (2021) 344–370, https://doi.org/10.1007/s12011-020-02138-3.
[19] A.A. Yaqoob, K. Umar, M.N.M. Ibrahim, Silver nanoparticles: various methods of synthesis, size affecting factors and their potential applications–a review, Appl. Nanosci. 10 (2020) 1369–1378, https://doi.org/10.1007/s13204-020-01318-w.
[20] N. Esmaili, P. Mohammadi, M. Abbaszadeh, H. Sheibani, Green synthesis of silver nanoparticles using Eucalyptus comadulensis leaves extract and its immobilization on magnetic nanocomposite (GO-Fe3O4/PAA/Ag) as a recoverable catalyst for degradation of organic dyes in water, Appl. Organomet. Chem. 34 (2020), e5547, https://doi.org/10.1002/aoc.5547.
[21] A.M. El Shafey, Green synthesis of metal and metal oxide nanoparticles from plant leaf extracts and their applications: a review, Green Process. Synth. 9 (2020) 304–339, https://doi.org/10.1515/gps-2020-0031.
[22] A. Saravanan, P.S. Kumar, S. Karishma, D.-V.N. Vo, S. Jeevanantham, P. R. Yaashikaa, C.S. George, A review on biosynthesis of metal nanoparticles and its environmental applications, Chemosphere 264 (2021), 128580, https://doi.org/10.1016/j.chemosphere.2020.128580.
[23] B. Siripireddy, B.K. Mandal, Facile green synthesis of zinc oxide nanoparticles by Eucalyptus globulus and their photocatalytic and antioxidant activity, Adv. Powder Technol. 28 (2017) 785–797, https://doi.org/10.1016/j.apt.2016.11.026.
[24] K. Cao, M.-M. Chen, F.-Y. Chang, Y.-Y. Cheng, L.-J. Tian, F. Li, G.-Z. Deng, C. Wu, The biosynthesis of cadmium selenide quantum dots by Rhodotorula mucilaginosa PA-1 for photocatalysis, Biochem. Eng. J. 156 (2020), 107497, https://doi.org/10.1016/j.bej.2020.107497.
[25] X. Xu, Y. Yang, H. Jin, B. Pang, C. Jiang, D. Shao, J. Shi, Filamentous fungal in situ biosynthesis of heterogeneous Au/Cd0.5Zn0.5S nano-photocatalyst: a macroscopic assembly strategy for preparing composite mycelial pellets with visible light degradation ability, J. Hazard. Mater. 406 (2021), 124797, https://doi.org/10.1016/j.jhazmat.2020.124797.
[26] K. Vijai Anand, J. Aravind Kumar, K. Keerthana, P. Deb, S. Tamilselvan, J. Theerthagiri, V. Rajeswari, S.M.S. Sekaran, K. Govindaraju, Photocatalytic degradation of rhodamine B dye using biogenic hybrid ZnO-MgO nanocomposites under visible light, ChemistrySelect 4 (2019) 5178–5184, https://doi.org/10.1002/slct.201900213.
[27] S. Shamaila, A.K.L. Sajjad, N.-A. Ryma, S.A. Farooqi, N. Jabeen, S. Majeed, I. Farooq, Advancements in nanoparticle fabrication by hazard free eco-friendly green routes, Appl. Mater. Today 5 (2016) 150–199, https://doi.org/10.1016/J.APMT.2016.09.009.
[28] M. Rahimi-Nasrabadi, S.M. Pourmortazavi, S.A.S. Shandiz, F. Ahmadi, H. Batooli, Green synthesis of silver nanoparticles using Eucalyptus leucoxylon leaves extract and evaluating the antioxidant activities of extract, Nat. Prod. Res. 28 (2014) 1964–1969, https://doi.org/10.1080/14786419.2014.918124.
[29] H. Sawalha, R. Abiri, R. Sanusi, N.A. Shaharuddin, A.A. Noor, N.A. Ab Shukor, H. Abdul-Hamid, S.A. Ahmad, Toward a better understanding of metal nanoparticles, a novel strategy from Eucalyptus plants, Plants 10 (2021), https://doi.org/10.3390/plants10050929.
[30] A.K. Chauhan, N. Kataria, V.K. Garg, Green fabrication of ZnO nanoparticles using Eucalyptus spp. leaves extract and their application in wastewater remediation, Chemosphere 247 (2020), 125803, https://doi.org/10.1016/j.chemosphere.2019.125803.
[31] N. Ramezani, Z. Ehsanfar, F. Shamsa, G. Amin, H.R. Shahverdi, H.R.M. Esfahani, A. Shamsaie, R.D. Bazaz, A.R. Shahverdi, Screening of Medicinal Plant Methanol Extracts for the Synthesis of Gold Nanoparticles by Their Reducing Potential 63, 2008, pp. 903–908, https://doi.org/10.1515/znb-2008-0715.
[32] Y. Liu, X. Jin, Z. Chen, The formation of iron nanoparticles by Eucalyptus leaf extract and used to remove Cr(VI), Sci. Total Environ. 627 (2018) 470–479, https://doi.org/10.1016/j.scitotenv.2018.01.241.
[33] M. Rabeea, M. Owaid, R. Muslim, Synthesis and characterization of silver nanoparticles by natural organic compounds extracted from Eucalyptus leaves and their role in the catalytic degradation of methylene blue dye, Songklanakarin, J. Sci. Technol. 43 (2021) 14–23, https://doi.org/10.14456/sjst-psu.2021.3.
[34] M. Hafeez, A. Ghazal, J. Khan, P. Ahmad, M.U. Khandaker, H. Osman, S. Alamri, Eucalyptus globulus extract-assisted fabrication of copper oxide/zinc oxide nanocomposite for photocatalytic applications, Crystals 12 (2022), https://doi.org/10.3390/cryst12081153.
[35] A.K. Chauhan, N. Kataria, R. Gupta, V.K. Garg, Biogenic fabrication of ZnO@EC and MgO@EC using Eucalyptus leaf extract for the removal of hexavalent chromium Cr(VI) ions from water, Environ. Sci. Pollut. Res. (2023), https://doi.org/10.1007/s11356-022-24967-6.
[36] X. Weng, M. Guo, F. Luo, Z. Chen, One-step green synthesis of bimetallic Fe/Ni nanoparticles by eucalyptus leaf extract: biomolecules identification, characterization and catalytic activity, Chem. Eng. J. 308 (2017) 904–911, https://doi.org/10.1016/j.cej.2016.09.134.
[37] Y. Lin, X. Jin, N.I. Khan, G. Owens, Z. Chen, Efficient removal of As (III) by calcined green synthesized bimetallic Fe/Pd nanoparticles based on adsorption and oxidation, J. Clean. Prod. 286 (2021), 124987, https://doi.org/10.1016/j.jclepro.2020.124987.
[38] R.D. Wouters, P.C.L. Muraro, D.M. Druzian, A.R. Viana, E. de Oliveira Pinto, J.K. L. da Silva, B.S. Vizzotto, Y.P.M. Ruiz, A. Galembeck, G. Pavoski, D.C.R. Espinosa, W.L. da Silva, Zinc oxide nanoparticles: biosynthesis, characterization, biological activity and photocatalytic degradation for tartrazine yellow dye, J. Mol. Liq. 371 (2023), 121090, https://doi.org/10.1016/j.molliq.2022.121090.
[39] E. Coelho, M. Lemos, Z. Genisheva, L. Domingues, M. Vilanova, J.M. Oliveira, Validation of a LLME/GC-MS methodology for quantification of volatile compounds in fermented beverages, Molecules 25 (2020), https://doi.org/10.3390/molecules25030621.
[40] P. Ferreira-Santos, R. Nunes, F. De Biasio, G. Spigno, D. Gorgoglione, J. A. Teixeira, C.M.R. Rocha, Influence of thermal and electrical effects of ohmic heating on C-phycocyanin properties and biocompounds recovery from Spirulina platensis, LWT 128 (2020), 109491, https://doi.org/10.1016/j.lwt.2020.109491.
[41] B. Sancey, G. Trunfio, J. Charles, J.-F. Minary, S. Gavoille, P.-M. Badot, G. Crini, Heavy metal removal from industrial effluents by sorption on cross-linked starch: chemical study and impact on water toxicity, J. Environ. Manage. 92 (2011) 765–772, https://doi.org/10.1016/j.jenvman.2010.10.033.
[42] K. Tanji, J.A. Navio, A. Chaqroune, J. Naja, F. Puga, M.C. Hidalgo, A. Kherbeche, Fast photodegradation of rhodamine B and caffeine using ZnO-hydroxyapatite composites under UV-light illumination, Catal. Today 388–389 (2022) 176–186, https://doi.org/10.1016/j.cattod.2020.07.044.
[43] C.V. Restrepo, C.C. Villa, Synthesis of silver nanoparticles, influence of capping agents, and dependence on size and shape: a review, Environ. Nanotechnol. Monit. Manag. 15 (2021), 100428, https://doi.org/10.1016/j.enmm.2021.100428.
[44] D. Baruah, M. Goswami, R.N.S. Yadav, A. Yadav, A.M. Das, Biogenic synthesis of gold nanoparticles and their application in photocatalytic degradation of toxic dyes, J. Photochem. Photobiol. B Biol. 186 (2018) 51–58, https://doi.org/10.1016/j.jphotobiol.2018.07.002.
[45] M.S. Kiran, V.S. Betageri, C.R.R. Kumar, S.P. Vinay, M.S. Latha, In-vitro antibacterial, antioxidant and cytotoxic potential of silver nanoparticles synthesized using novel Eucalyptus tereticornis leaves extract, J. Inorg. Organomet. Polym. Mater. 30 (2020) 2916–2925, https://doi.org/10.1007/s10904-020-01443-7.
[46] V. Vilas, D. Philip, J. Mathew, Catalytically and biologically active silver nanoparticles synthesized using essential oil, Spectrochim. Acta A Mol. Biomol. Spectrosc. 132 (2014) 743–750, https://doi.org/10.1016/j.saa.2014.05.046.
[47] L.M. Liz-Marzán, Tailoring surface plasmons through the morphology and assembly of metal nanoparticles, Langmuir 22 (2006) 32–41, https://doi.org/10.1021/la0513353.
[48] I. Alghoraibi, C. Soukkarieh, R. Zein, A. Alahmad, J.-G. Walter, M. Daghestani, Aqueous extract of Eucalyptus camaldulensis leaves as reducing and capping agent in biosynthesis of silver nanoparticles, Inorg. Nano-Metal Chem. 50 (2020) 895–902, https://doi.org/10.1080/24701556.2020.1728315.
[49] R.T.V. Vimala, G. Sathishkumar, S. Sivaramakrishnan, Optimization of reaction conditions to fabricate nano-silver using *Couroupita guianensis* Aubl. (leaf & fruit) and its enhanced larvicidal effect, Spectrochim. Acta A Mol. Biomol. Spectrosc. 135 (2015) 110–115, https://doi.org/10.1016/j.saa.2014.06.009.
[50] S. Patil, R. Chandrasekaran, Biogenic nanoparticles: a comprehensive perspective in synthesis, characterization, application and its challenges, J. Genet. Eng. Biotechnol. 18 (2020) 67, https://doi.org/10.1186/s43141-020-00081-3.
[51] M.F. Zayed, W.H. Eisa, Phoenix dactylifera L. leaf extract phytosynthesized gold nanoparticles; controlled synthesis and catalytic activity, Spectrochim. Acta A Mol. Biomol. Spectrosc. 121 (2014) 238–244, https://doi.org/10.1016/j.saa.2013.10.092.
[52] R.J.B. Pinto, J.M.F. Lucas, M.P. Morais, S.A.O. Santos, A.J.D. Silvestre, P.A.A. P. Marques, C.S.R. Freire, Demystifying the morphology and size control on the biosynthesis of gold nanoparticles using Eucalyptus globulus bark extract, Ind. Crop. Prod. 105 (2017) 83–92, https://doi.org/10.1016/j.indcrop.2017.05.003.
[53] M. Valodkar, P.S. Nagar, R.N. Jadeja, M.C. Thounaojam, R.V. Devkar, S. Thakore, Euphorbiaceae latex induced green synthesis of non-cytotoxic metallic nanoparticle solutions: a rational approach to antimicrobial applications, Colloids Surf. A Physicochem. Eng. Asp. 384 (2011) 337–344, https://doi.org/10.1016/j.colsurfa.2011.04.015.
[54] P. Ferreira-Santos, Z. Genisheva, C. Botelho, J. Santos, C. Ramos, J.A. Teixeira, C. M.R. Rocha, Unravelling the biological potential of Pinus pinaster bark extracts, Antioxidants (Basel, Switzerland) 9 (2020) 334, https://doi.org/10.3390/antiox9040334.
[55] A.C. Dong, P. Huang, B. Caughey, W.S. Caughey, Infrared analysis of ligand- and oxidation-induced conformational changes in hemoglobins and myoglobins, Arch. Biochem. Biophys. 316 (1995) 893–898, https://doi.org/10.1006/abbi.1995.1120.
[56] K.J. Brobbey, J. Haapanen, M. Gunell, M. Toivakka, J.M. Mäkelä, E. Eerola, R. Ali, M.R. Saleem, S. Honkanen, J. Bobacka, J.J. Saarinen, Controlled time release and leaching of silver nanoparticles using a thin immobilizing layer of aluminum oxide, Thin Solid Films 645 (2018) 166–172, https://doi.org/10.1016/j.tsf.2017.09.060.

[57] J.F. Moulder, Handbook of X-ray Photoelectron Spectroscopy: A Reference Book of Standard Spectra for Identification and Interpretation of XPS Data, Physical Electronics Division, Perkin-Elmer Corporation, 1992.
[58] A.M. Fonseca, I.C. Neves, Study of silver species stabilized in different microporous zeolites, Microporous Mesoporous Mater. 181 (2013) 83–87, https://doi.org/10.1016/j.micromeso.2013.07.018.
[59] A.V. Naumkin, A. Kraut-Vass, S.W. Gaarenstroom, C.J. Powell, NIST X-ray Photoelectron Spectroscopy Database, NIST Stand. Ref. Database 20, Version 4.1, 2012.
[60] J.P.Z. Gonçalves, J. Seraglio, D.L.P. Macuvele, N. Padoin, C. Soares, H.G. Riella, Green synthesis of manganese based nanoparticles mediated by Eucalyptus robusta and Corymbia citriodora for agricultural applications, Colloids Surf. A Physicochem. Eng. Asp. 636 (2022), 128180, https://doi.org/10.1016/j.colsurfa.2021.128180.
[61] M. Sivagami, I.V. Asharani, Catalytic reduction of nitroarenes by Cucumis maderaspatanus L. leaves extract mediated silver nanoparticles, J. Taiwan Inst. Chem. Eng. 149 (2023), 104981, https://doi.org/10.1016/j.jtice.2023.104981.
[62] Z. Gharari, P. Hanachi, H. Sadeghinia, T.R. Walker, Eco-friendly green synthesis and characterization of silver nanoparticles by Scutellaria multicaulis leaf extract and its biological activities, Pharmaceuticals 16 (2023), https://doi.org/10.3390/ph16070992.
[63] J. Jiang, G. Oberdörster, A. Elder, R. Gelein, P. Mercer, P. Biswas, Does nanoparticle activity depend upon size and crystal phase? Nanotoxicology 2 (2008) 33–42, https://doi.org/10.1080/17435390701882478.
[64] Y. Mo, Y. Tang, S. Wang, J. Lin, H. Zhang, D. Luo, Green synthesis of silver nanoparticles using eucalyptus leaf extract, Mater. Lett. 144 (2015) 165–167, https://doi.org/10.1016/j.matlet.2015.01.004.
[65] S.A.O. Santos, R.J.B. Pinto, S.M. Rocha, P.A.A.P. Marques, C.P. Neto, A.J. D. Silvestre, C.S.R. Freire, Unveiling the chemistry behind the green synthesis of metal nanoparticles, ChemSusChem 7 (2014) 2704–2711, https://doi.org/10.1002/cssc.201402126.
[66] M. Khatun, Z. Khatun, M.R. Karim, M.R. Habib, M.H. Rahman, M.A. Aziz, Green synthesis of silver nanoparticles using extracts of Mikania cordata leaves and evaluation of their antioxidant, antimicrobial and cytotoxic properties, Food Chem. Adv. 3 (2023), 100386, https://doi.org/10.1016/j.focha.2023.100386.
[67] S.M. Roopan, G. Rohit, A.A. Madhumitha, C. Rahuman, A. Kamaraj, T. V. Bharathi, Surendra, low-cost and eco-friendly phyto-synthesis of silver nanoparticles using Cocos nucifera coir extract and its larvicidal activity, Ind. Crop. Prod. 43 (2013) 631–635, https://doi.org/10.1016/j.indcrop.2012.08.013.
[68] S. Jebril, A. Fdhila, C. Dridi, Nanoengineering of eco-friendly silver nanoparticles using five different plant extracts and development of cost-effective phenol nanosensor, Sci. Rep. 11 (2021) 22060, https://doi.org/10.1038/s41598-021-01609-4.
[69] D. Ben Hassine, R. Rahmani, J.P. Souchard, M. Abderrabba, J. Bouajila, Eucalyptus brevifolia F., Muell and Eucalyptus stricklandii maiden leaves extracts: HPLC-DAD, GC-MS analysis and in vitro biological activities, combined with the principal component analysis, S. Afr. J. Bot. 147 (2022) 826–839, https://doi.org/10.1016/j.sajb.2022.03.027.
[70] Z. Obeizi, H. Benbouzid, S. Ouchenane, D. Yılmaz, M. Culha, M. Bououdina, Biosynthesis of zinc oxide nanoparticles from essential oil of Eucalyptus globulus with antimicrobial and anti-biofilm activities, Mater. Today Commun. 25 (2020), 101553, https://doi.org/10.1016/j.mtcomm.2020.101553.
[71] A. Ashraf, R.A. Sarfraz, A. Mahmood, M. Ud Din, Chemical composition and in vitro antioxidant and antitumor activities of Eucalyptus camaldulensis Dehn. leaves, Ind. Crop. Prod. 74 (2015) 241–248, https://doi.org/10.1016/j.indcrop.2015.04.059.
[72] I. Almas, E. Innocent, F. Machumi, W. Kisinza, Chemical composition of essential oils from Eucalyptus globulus and Eucalyptus maculata grown in Tanzania, Sci. Afr. 12 (2021), e00758, https://doi.org/10.1016/j.sciaf.2021.e00758.
[73] Z.-R. Mashwani, M.A. Khan, T. Khan, A. Nadhman, Applications of plant terpenoids in the synthesis of colloidal silver nanoparticles, Adv. Colloid Interface Sci. 234 (2016) 132–141, https://doi.org/10.1016/j.cis.2016.04.008.
[74] J.Y. Song, B.S. Kim, Rapid biological synthesis of silver nanoparticles using plant leaf extracts, Bioprocess Biosyst. Eng. 32 (2009) 79–84, https://doi.org/10.1007/s00449-008-0224-6.
[75] K. Wang, Y. Liu, X. Jin, Z. Chen, Characterization of iron nanoparticles/reduced graphene oxide composites synthesized by one step eucalyptus leaf extract, Environ. Pollut. 250 (2019) 8–13, https://doi.org/10.1016/j.envpol.2019.04.002.
[76] K. Ali, B. Ahmed, S.M. Ansari, Q. Saquib, A.A. Al-Khedhairy, S. Dwivedi, M. Alshaeri, M.S. Khan, J. Musarrat, Comparative in situ ROS mediated killing of bacteria with bulk analogue, Eucalyptus leaf extract (ELE)-capped and bare surface copper oxide nanoparticles, Mater. Sci. Eng. C 100 (2019) 747–758, https://doi.org/10.1016/j.msec.2019.03.012.
[77] T.J.I. Edison, M.G. Sethuraman, Instant green synthesis of silver nanoparticles using Terminalia chebula fruit extract and evaluation of their catalytic activity on reduction of methylene blue, Process Biochem. 47 (2012) 1351–1357, https://doi.org/10.1016/j.procbio.2012.04.025.
[78] A.K. Mittal, S. Kumar, U.C. Banerjee, Quercetin and gallic acid mediated synthesis of bimetallic (silver and selenium) nanoparticles and their antitumor and antimicrobial potential, J. Colloid Interface Sci. 431 (2014) 194–199, https://doi.org/10.1016/j.jcis.2014.06.030.
[79] M. Pradeep, D. Kruszka, P. Kachlicki, D. Mondal, G. Franklin, Uncovering the phytochemical basis and the mechanism of plant extract-mediated eco-friendly synthesis of silver nanoparticles using ultra-performance liquid chromatography coupled with a photodiode array and high-resolution mass spectrometry, ACS Sustain. Chem. Eng. 10 (2022) 562–571, https://doi.org/10.1021/acssuschemeng.1c06960.
[80] S. Jain, M.S. Mehata, Medicinal plant leaf extract and pure flavonoid mediated green synthesis of silver nanoparticles and their enhanced antibacterial property, Sci. Rep. 7 (2017) 15867, https://doi.org/10.1038/s41598-017-15724-8.
[81] S.M. Ghoreishi, M. Behpour, M. Khayatkashani, Green synthesis of silver and gold nanoparticles using Rosa damascena and its primary application in electrochemistry, Phys. E Low-Dimen. Syst. Nanostruct. 44 (2011) 97–104, https://doi.org/10.1016/j.physe.2011.07.008.
[82] A. Abdal Dayem, M.K. Hossain, S.B. Lee, K. Kim, S.K. Saha, G.-M. Yang, H.Y. Choi, S.-G. Cho, The role of reactive oxygen species (ROS) in the biological activities of metallic nanoparticles, Int. J. Mol. Sci. 18 (2017), https://doi.org/10.3390/ijms18010120.
[83] M.M.K. Peiris, S.S.N. Fernando, P.M. Jayaweera, N.D.H. Arachchi, T.D.C. P. Guansekara, Comparison of antimicrobial properties of silver nanoparticles synthesized from selected bacteria, Indian J. Microbiol. 58 (2018) 301–311, https://doi.org/10.1007/s12088-018-0723-3.
[84] B. Bhuyan, A. Paul, B. Paul, S.S. Dhar, P. Dutta, Paederia foetida Linn. promoted biogenic gold and silver nanoparticles: synthesis, characterization, photocatalytic and in vitro efficacy against clinically isolated pathogens, J. Photochem. Photobiol. B Biol. 173 (2017) 210–215, https://doi.org/10.1016/j.jphotobiol.2017.05.040.
[85] G. Franci, A. Falanga, S. Galdiero, L. Palomba, M. Rai, G. Morelli, M. Galdiero, Silver nanoparticles as potential antibacterial agents, Molecules 20 (2015) 8856–8874, https://doi.org/10.3390/molecules20058856.
[86] M. Mehta, M. Sharma, K. Pathania, P.K. Jena, I. Bhushan, Degradation of synthetic dyes using nanoparticles: a mini-review, Environ. Sci. Pollut. Res. 28 (2021) 49434–49446, https://doi.org/10.1007/s11356-021-15470-5.
[87] W.M. Shume, H.C.A. Murthy, E.A. Zereffa, A review on synthesis and characterization of Ag_2O nanoparticles for photocatalytic applications, J. Chem. 2020 (2020), 5039479, https://doi.org/10.1155/2020/5039479.
[88] Ruby Aryan, M.S. Mehata, Green synthesis of silver nanoparticles using Kalanchoe pinnata leaves (life plant) and their antibacterial and photocatalytic activities, Chem. Phys. Lett. 778 (2021), 138760, https://doi.org/10.1016/j.cplett.2021.138760.
[89] S.Y. Janbandhu, U. Patra, G.K. Sukhadeve, R. Kumar, R.S. Gedam, Photocatalytic performance of glasses embedded with Ag-TiO2 quantum dots on photodegradation of indigo carmine and eosin Y dyes in sunlight, Inorg. Chem. Commun. 148 (2023), 110317, https://doi.org/10.1016/j.inoche.2022.110317.
[90] G.K. Sukhadeve, S.Y. Janbandhu, R. Kumar, D.H. Lataye, D.D. Ramteke, R. S. Gedam, Visible light assisted photocatalytic degradation of indigo carmine dye and NO2 removal by Fe doped TiO2 nanoparticles, Ceram. Int. 48 (2022) 29121–29135, https://doi.org/10.1016/j.ceramint.2022.05.053.
[91] A. Khiari MickaëlAU - Lejeune, MichaëlAU - Lazar, FloricaAU - Hadjadj, Effects of Ag nanoparticles on zinc oxide photocatalytic performance, Coatings 11 (2021), https://doi.org/10.3390/coatings11040400.
[92] G. Gyawali, R. Adhikari, B. Joshi, T.H. Kim, V. Rodríguez-González, S.W. Lee, Sonochemical synthesis of solar-light-driven Ag̊-PbMoO4 photocatalyst, J. Hazard. Mater. 263 (2013) 45–51, https://doi.org/10.1016/j.jhazmat.2013.03.065.
[93] T.T. Guaraldo, T.B. Zanoni, S.I.C. de Torresi, V.R. Gonçales, G.J. Zocolo, D. P. Oliveira, M.V.B. Zanoni, On the application of nanostructured electrodes prepared by Ti/TiO2/WO3 “template”: a case study of removing toxicity of indigo using visible irradiation, Chemosphere 91 (2013) 586–593, https://doi.org/10.1016/j.chemosphere.2012.12.027.
[94] A. Hernández-Gordillo, V. Rodríguez-González, S. Oros-Ruiz, R. Gómez, Photodegradation of indigo carmine dye by CdS nanostructures under blue-light irradiation emitted by LEDs, Catal. Today 266 (2016) 27–35, https://doi.org/10.1016/j.cattod.2015.09.001.
[95] V. Aleksic Sabo, P. Knezevic, Antimicrobial activity of Eucalyptus camaldulensis Dehn. plant extracts and essential oils: a review, Ind. Crop. Prod. 132 (2019) 413–429, https://doi.org/10.1016/j.indcrop.2019.02.051.
[96] K. Sebei, F. Sakouhi, W. Herchi, M.L. Khouja, S. Boukhchina, Chemical composition and antibacterial activities of seven Eucalyptus species essential oils leaves, Biol. Res. 48 (2015) 7, https://doi.org/10.1186/0717-6287-48-7.
[97] G. Dogan, N. Kara, E. Bagci, S. Gur, Chemical composition and biological activities of leaf and fruit essential oils from Eucalyptus camaldulensis, Z. Naturforsch. C 72 (2017) 483–489, https://doi.org/10.1515/znc-2016-0033.
[98] L. Zhou, J. Li, Q. Kong, S. Luo, J. Wang, S. Feng, M. Yuan, T. Chen, S. Yuan, C. Ding, Chemical composition, antioxidant, antimicrobial, and phytotoxic potential of Eucalyptus grandis × E. urophylla leaves essential oils, Molecules 26 (2021), https://doi.org/10.3390/molecules26051450.
[99] D. Ben Hassine, M. Abderrabba, Y. Yvon, A. Lebrihi, F. Mathieu, F. Couderc, J. Bouajila, Chemical composition and in vitro evaluation of the antioxidant and antimicrobial activities of Eucalyptus gillii essential oil and extracts, Molecules 17 (2012) 9540–9558, https://doi.org/10.3390/molecules17089540.
[100] S. Diloksumpun, N. Wongkattiya, K. Buaban, T. Saleepochn, P. Suttiarporn, S. Luangkamin, Variation in the antibacterial and antioxidant activities of essential oils of five new Eucalyptus urophylla S.T. Blake clones in Thailand, Molecules 27 (2022), https://doi.org/10.3390/molecules27030680.
[101] Y. Huang, M. An, A. Fang, O.J. Olatunji, F.N. Eze, Antiproliferative activities of the lipophilic fraction of Eucalyptus camaldulensis against MCF-7 breast cancer cells, UPLC-ESI-QTOF-MS metabolite profile, and antioxidative functions, ACS Omega 7 (2022) 27369–27381, https://doi.org/10.1021/acsomega.2c02389.

[102] M. Pan, Q. Lei, H. Zhang, Prediction and confirmation of active ingredients in Eucalyptus globulus Labill leaves, Ind. Crop. Prod. 154 (2020), 112631, https://doi.org/10.1016/j.indcrop.2020.112631.
[103] Y. Amakura, M. Yoshimura, N. Sugimoto, T. Yamazaki, T. Yoshida, Marker constituents of the natural antioxidant eucalyptus leaf extract for the evaluation of food additives, Biosci. Biotechnol. Biochem. 73 (2009) 1060–1065, https://doi.org/10.1271/bbb.80832.
[104] Dezsi Ștefan, A.S. Bădărău, C. Bischin, D.C. Vodnar, R. Silaghi-Dumitrescu, A.-M. Gheldiu, A. Mocan, L. Vlase, Antimicrobial and antioxidant activities and phenolic profile of *Eucalyptus globulus* Labill. and *Corymbia ficifolia* (F. Muell.) K. D. Hill & L.A.S. Johnson Leaves, Molecules 20 (2015) 4720–4734, https://doi.org/10.3390/molecules20034720.
[105] C. Ferreiraa, A. Pereyrab, A. Patriarcaa, M. Mazzobrea, T. Polak, V. Abram, M. Bueraa, N. PoklarUlrihd, Phenolic compounds in extracts from Eucalyptus globulus leaves and Calendula officinalis flowers, J. Nat. Prod. Res. 2 (1) (2016) 53–57 (www.jacsdi).
[106] A. Nasr, T. Saleem Khan, G.-P. Zhu, Phenolic compounds and antioxidants from Eucalyptus camaldulensis as affected by some extraction conditions, a preparative optimization for GC-MS analysis, Prep. Biochem. Biotechnol. 49 (2019) 464–476, https://doi.org/10.1080/10826068.2019.1575860.
[107] E. Al-Sayed, A.-N. Singab, N. Ayoub, O. Martiskainen, J. Sinkkonen, K. Pihlaja, HPLC–PDA–ESI–MS/MS profiling and chemopreventive potential of Eucalyptus gomphocephala DC, Food Chem. 133 (2012) 1017–1024, https://doi.org/10.1016/j.foodchem.2011.09.036.
[108] F. Gomes, N. Martins, L. Barros, M.E. Rodrigues, M.B.P.P. Oliveira, M. Henriques, I.C.F.R. Ferreira, Plant phenolic extracts as an effective strategy to control Staphylococcus aureus, the dairy industry pathogen, Ind. Crop. Prod. 112 (2018) 515–520, https://doi.org/10.1016/j.indcrop.2017.12.027.
[109] L. Boulekbache-Makhlouf, E. Meudec, J.-P. Mazauric, K. Madani, V. Cheynier, Qualitative and semi-quantitative analysis of phenolics in eucalyptus globulus leaves by high-performance liquid chromatography coupled with diode array detection and electrospray ionisation mass spectrometry, Phytochem. Anal. 24 (2013) 162–170, https://doi.org/10.1002/pca.2396.
[110] M.A. Ghareeb, M.R. Habib, H.S. Mossalem, M.S. Abdel-Aziz, Phytochemical analysis of Eucalyptus camaldulensis leaves extracts and testing its antimicrobial and schistosomicidal activities, Bull. Natl. Res. Cent. 42 (2018) 16, https://doi.org/10.1186/s42269-018-0017-2.